SFRC exposed to high temperature: Hot vs. residual characterization for thin walled elements

Matteo Colombo, Marco di Prisco *, Roberto Felicetti

Department of Civil and Environmental Engineering, Politecnico di Milano, 20133 Milano, Italy

Received 28 March 2014
Received in revised form 10 November 2014
Accepted 5 January 2015
Available online 12 January 2015

1. Introduction

Steel fibers improve the mechanical performance of concrete and represent a promising solution, especially with reference to the bending of thin-walled elements. Their use in prefabricated roof elements can be considered interesting from the economical point of view as an alternative to welded-wire mesh and tradi-tional distributed reinforcement once the ductility of structure response is guaranteed [1–3]. Moreover, the correct positioning of the reinforcement suggested by a careful durability design can be hardly guaranteed in thin sections, and therefore fiber reinforcement seems very effective. The main advantages associated with its use can be summarized in better controlled quality, thickness reduction (no cover limitations), greater design freedom in sketching the cross-section profile, prevention of complex reinforcement detailing, more industrialized production with a strong reduction of man-activity in the reinforcement arrangement (no mesh handling and placing), better spread and continuously adjustable reinforcement, and, finally, no need for a tolerance check on the reinforcement position. Some very significant appli-cations in architecture have also combined continuous reinforce-ment meshes with fiber-reinforced cementitious composites in order to obtain a controlled membrane strength associated with a significant bending strength [2,4]. Other authors have suggested fiber-reinforced thin-walled elements as sheet piles [5].

Steel macro-fibers significantly modify uniaxial tension behavior by means of pull-out mechanism [6–8]: the post-cracking strength is affected by several parameters related to the fiber adopted, like bond strength, type, geometry, aspect ratio, content, and steel strength, and to the casting procedure, like dispersion and orientation in volume and matrix mechanical characteristics. These aspects interact in a quite complex way and, for this reason, the actual recommendations suggest considering the material as a composite with mechanical characteristics affected by a certain standard deviation [3]. This approach also implies a design based on material performance. A bending test is the easiest method of mechanical characterization [9], because a uniaxial tension test is more sensible to boundary conditions and requires test facilities not common in experimental laboratories. In the literature, a careful check on the reliability of the bending test as a reference test for the identification of uniaxial tension behavior, was also carried out [10]. Of course, two main doubts can be explored. The former is related to the random fiber dispersion: the material can be assimilated to a homogeneous material if any evident accumulation of fibers is prevented despite the significant difference in terms of density between diffused reinforcement and paste. The latter is related to the pull-out mechanism: during crack propagation, local curvature due to bending can introduce a second-order confinement pressure that could increase the flexural strength at high crack opening values. When fiber segregation is prevented, the difference between bending and uniaxial tension in terms of toughness can reach about 20% [11], if a significant steel macro-fiber content is used (>0.5% by volume). The comparison is meaningful

* Corresponding author. Tel.: +39 0223998794; fax: +39 0223998771.
E-mail address: marco.diprisco@polimi.it (M. di Prisco).

only if the specimens are tested taking into account the casting and vibration directions with respect to the stretching one [12]. As far as thin-walled elements are concerned [13], several experimental results have shown that the most reliable bending test is the unnotched one [10], because different parameters, like the casting procedure, wall effects, fiber shape, and matrix consistency, can affect the post-peak strength with respect to what is expected from theoretical prediction, as suggested by Soroushian and Lee [14]. Of course, a check of the topological homogeneity of the material in the structure by means of suitable controls at the fresh and hard-ened states [15] is also strongly suggested. This check guarantees the representativeness of the single specimen with reference to the structural behavior at room condition, but also when exposed to high temperature.

Looking at thermo-mechanical behavior, mechanical characterization at high temperature is possible, but this kind of test requires suitable mechanical devices not readily available in a lab-oratory [16,17]. In order to overcome this difficulty, in the litera-ture two main experimental procedures are proposed for concrete characterization. The former applies a load to the speci-men at room temperature after previous exposure to a high tem-perature, according to a thermal cycle aimed at favoring homogeneous damage in the material by means of a very low tem-perature rate [16,18]. The latter applies a load to a hot specimen, trying to reduce the test time as much as possible, in order to dis-regard the specimen's cooling [19]. Further procedures apply stan-dard fire temperature vs. time curves directly to the specimen used to identify the material properties [20] preventing, in this way, the uncoupling between the mechanical properties evolution with temperature grow from the structural effect imposed by boundary conditions.

Few papers have investigated the evolution of the toughness with temperature growth. In these cases [20] the evolution is described in terms of toughness indexes coupling the post-crack-ing properties with the elastic ones, often without a clear trend with increasing temperature and very few information about sta-tistical distribution.

Other papers [21–23] investigated the sensitivity of the com-pressive behavior of SFRC to high temperature thus excluding the only mechanical contribution that Model Code 2010 recognizes to the fiber reinforcement.

A comprehensive research project on the structural applica-tions of SFRC has been carried out, in cooperation with a precast Industry, in order to ascertain the effects of partial – or even total – replacement of the traditional steel reinforcement in some spe-cific structural members [24]. Previous results on high tempera-ture resistance of SFRC plates [25] show comparable behavior with R/C plates characterized by the same steel content. This practice can also be regarded as a smart mean to enhance struc-tural performance under extreme environmental conditions, such as fire exposure. Within this framework and according to codes on fire design [26,27], this study is aimed at assessing the param-eters needed for the thermal and mechanical analysis of SFRC structural members, in the case of fire design. Due to the simplic-ity of identifying residual strength after thermal cycles, the research was also oriented to quantify the difference obtainable by measuring the material response at a high temperature (hot behavior) or after cooling down to room temperature (residual behavior).

A previous investigation has shown that the small fiber volume percentage introduced does not affect the thermal properties of the cement based composite [28]. In a following paper [29] aimed at analysing the behavior of a SFRC material tested according to Stan-dard classification, authors have shown how it is possible to char-acterize the thermal post-cracking strength degradation by means of notched bending tests by comparing the results with uniaxial tension tests performed on cylindrical specimens directly cored from the same prismatic beam used for notched bending tests.

Focusing the attention to thin walled elements as regards high temperature behavior, the main objectives related to steel fiber reinforced concrete can be summarized as follows:

(a) Difference between hot and residual tests in the identifica-tion of the mechanical strengths degradation for a SFRC exposed to high temperature in thin-walled elements.
(b) Evaluation of the high temperature influence on first and post cracking equivalent strengths also in comparison with plain concrete tensile strength.
(c) Existence of a unique degradation function not dependent on the specific SFRC analysed or need for a proper identifica-tion for each specific material.
(d) Prevailing failure mechanism in bending in hot and residual conditions (Pull-out or steel fiber failure).
(e) Effect of high temperature on the ductility associated to the global bending response of SFRC.

In order to clarify these points, an experimental investigation was carried out at the Magnetti Building laboratory in cooperation with the Politecnico di Milano. Four point bending tests were per-formed both on hot specimens, just extracted from the oven (as proposed by Pimienta in compressive tests [19]), and after cooling.

2. Research significance

Fire resistance is one of the most severe conditions to be consid-ered for thin-walled structural elements. Steel fiber reinforced con-crete (SFRC) requires a mechanical characterization performed by means of bending tests on a notched or unnotched specimen. The same mechanical characterization procedure can also be applied to thermally damaged specimens. In the experimental campaign presented in this paper, the authors refer to thin-walled elements for which unnotched bending tests are considered more reliable and identify residual thermal degradation of the main mechanical parameters, checking also if the thermal strength deg-radation measured after cooling is comparable with that measured at hot condition. This comparison is extended to four materials already proposed in prefabrication in order to show how the spe-cific mix design involves a different evolution of the mechanical parameters with temperature growth.

3. Materials and methods

In the experimental research four materials were investigated. The main variables considered are: matrix strength (f_{cc} = 40 and 75 MPa), steel fiber content (35 and 50 kg/m^3), and hooked-end steel fiber type (low carbon – aspect ratio l_f/d_f = 45, f_{tk} = 1300 MPa; high carbon – l_f/d_f = 80, f_{tk} = 2300 MPa, both 30 mm long). Follow-ing the scheme f_{cc}/fiber content/aspect ratio, these materials are denoted as follows: T75/50/45, T75/50/80, T40/50/45, and T40/ 35/45. The mix design of the materials investigated is summarized in Table 1.

Four point bending tests on unnotched specimens were per-formed on the materials after thermal treatment up to different temperatures (200, 400, 600 and 800 °C). For each material and for each temperature, both hot and residual testing conditions were adopted: in the former case the specimens were extracted from the furnace once reached the maximum temperature consid-ered and then immediately tested within an insulated environ-ment (fast extraction technique [19]) while in the latter case the specimens were tested after a cooling phase within the furnace down to room temperature (20 °C).

Table 1
Mix design of the materials investigated.

Constituent		Unit	T40/35/45	T40/50/45	T75/50/45	T75/50/80
Cement CEM I 52.5R		kg/m^3	300	300	380	380
Fly ash		kg/m^3	80	80	60	60
Siliceous aggregate	0–3 mm	kg/m^3	/	/	120	120
	0–12 mm		1450	1450	920	920
	3–6 mm		420	420	/	/
	8–15 mm		/	/	865	865
Plasticizer		l/m^3	6 (naphthalene sulphonate)	6 (naphthalene sulphonate)	3.5 (Acrylic)	3.5 (Acrylic)
Water		l/m^3	175		150	150
Fiber length		mm	30	30	30	30
Fiber aspect ratio			45	45	45	80
Fiber type			Hooked end Low carbon	Hooked end Low carbon	Hooked end High carbon	Hooked end High carbon
Fiber content		kg/m^3	35	50	50	50

In the experimental research the specimens adopted were prismatic, 500 mm long and with a 75 × 60 mm cross section (Fig. 1), and were prepared by sawing a 500 mm × 600 mm plate, 60 mm thick, in order to reproduce the fiber orientation as in thin-walled precast members. The plate was cast in a prefabrication plant taking the mould horizontal and by using a suitable hopper, characterized by a width of about 60 cm, moving along the longest axis of the slab; the plate was then cured for 28 days in water after when the specimens were sawn. Cutting the plate in a relatively small-sized specimen asks for some consideration on the expected experimental scattering. Former tests on the fiber content of cylinders of different diameters cored from thin plates produced with similar procedures [15] showed that for a 68 mm diameter the standard deviation is about ±10% and the average value is about 2% lower than the nominal one. Thanks to the comparable cross-section area, these results can be extended to the prismatic beams tested herein.

The bending tests were carried out using a closed-loop electromechanical press (INSTRON 5587; maximum load capacity of 30 kN; load precision: 0.4% of read value for load larger than 0.3 kN and 0.5% of read value for load smaller than 0.3 kN; crosshead displacement precision: 0.05% of read value) by controlling the crosshead displacement δ (Fig. 1). The steel loading device was directly connected to the machine and the load was balanced at the beginning of each test.

Besides the reference tests at room temperature (T = 20 °C), four temperatures were investigated for each material (T = 200, 400, 600, and 800 °C), either in residual (R) or in hot (H) conditions.

In both cases, the heating process was performed on the 500 × 75 × 60mm^3 prismatic specimens in subsequent steps by respecting an average heating rate < 1 °C/min followed by a 2-h stabilization phase at the maximum temperature. For the residual tests, the cooling process was governed by the natural cooling into the closed furnace.

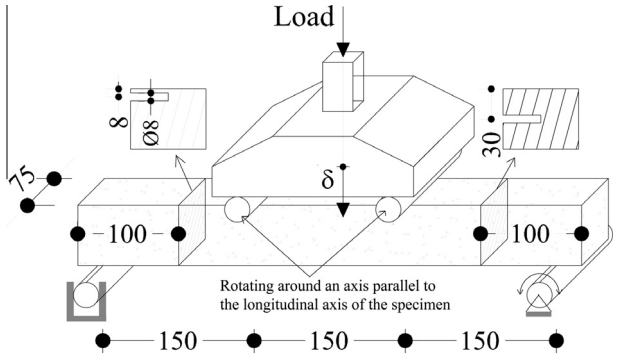

Fig. 1. Specimen geometry and load scheme.

The furnace used is an electrical furnace able to reach a maximum temperature of 1100 °C, with a power of 23 kW and with an internal chamber of dimensions 700 × 400 × 300 mm.

For the hot tests, the specimen was extracted from the hot furnace and placed on the test bench, within an insulating box. In order to prevent excessive cooling of the specimen, the tests were performed at relatively high displacement rates (1 mm/min and 2 mm/min for the pre- and the post-peak branches, respectively; denoted as "fast" in the follow). The influence of the displacement rate on the material behavior was investigated in a group of tests at room temperature carried out by imposing a displacement rate close to that suggested in EN 14651 and UNI 11188 (0.1 mm/min up to δ = 1.5 mm, 0.25 mm/min in the next 1.5 mm, and 0.5 mm/min in the final phase; denoted as "slow" in the follow). In the tests characterized by a low stroke rate in the room condition, two displacement transducers (Fig. 2b) were placed on the lateral side of the specimen along the bottom corner with a gauge length equal to 200 mm astride the constant bending moment region in order to measure the crack opening displacement on both sides of the specimen itself.

The temperature of the material during the high stroke rate tests was measured by means of two thermocouples inserted in as many 8 mm diameter holes drilled into each specimen (Figs. 1 and 2a). Given the difficulties of handling the hot specimen within a short period of time, no transducers were installed in all the tests with a high stroke rate. Hence, the crack opening displacement was evaluated using the two rigid bodies assumption after cracking, based on the displacement δ and on the actual crack position. It is worth noting that in the whole set of tests only one crack unsta-bly propagated in the critical zone.

As for the repeatability, three nominally identical tests for each case were carried out; the only exceptions were the tests with a low stroke rate for which only two nominally identical tests were carried out.

4. Thermal analysis

In the case of hot tests, in which the specimen is extracted from the furnace at temperature T_0 and suddenly exposed to the laboratory environment (T_{amb}), some doubts might arise about the actual material temperature during testing and about the effects of the self-stresses caused by the marked thermal gradients.

In order to investigate the thermal transient of a rectangular cross-section ($2a \times 2b$), the following governing equations, boundary and initial conditions were considered:

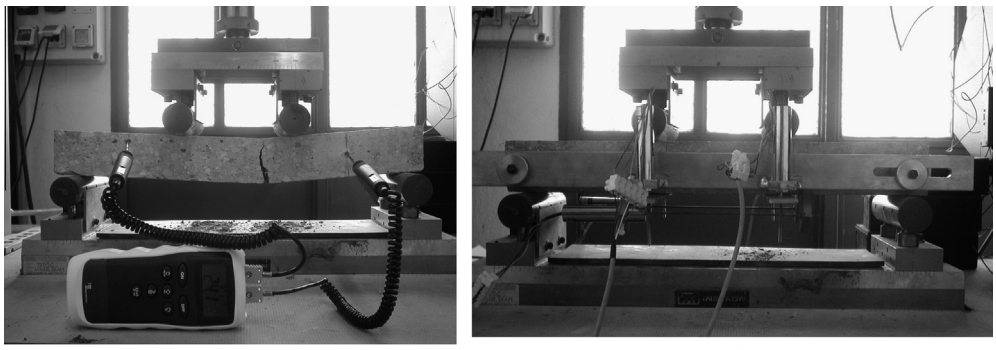

(a) (b)

Fig. 2. Test view: (a) hot and residual test set-up with typical crack pattern at failure and (b) slow test at room temperature.

$$\frac{\partial^2 T}{\partial x^2}+\frac{\partial^2 T}{\partial y^2}=\frac{1}{D}\frac{\partial T}{\partial t} \tag{1a}$$

where $D=\dfrac{\lambda}{\rho c}$ (D = thermal diffusivity; λ = thermal conductivity; ρ = density; c = specific heat)

$$-\lambda\frac{\partial T}{\partial x}+h\cdot(T-T_{amb})=0 \quad \text{for } x=-a \text{ and for } x=a \tag{1b}$$

$$-\lambda\frac{\partial T}{\partial y}+h\cdot(T-T_{amb})=0 \quad \text{for } y=-b \text{ and for } y=b \tag{1c}$$

$$T=T_0 \quad \forall x,y \text{ at } t=0 \tag{1d}$$

An analytical solution was worked out and several 1D finite difference and 2D finite element analyses were performed in order to validate it. Thanks to the limited temperature range involved during a few minutes cooling phase, some assumptions are allowable:

- Concrete thermal properties are governed by the maximum temperature T_0 experienced by the material and can be regarded as constants thereafter. No heat sources or sinks have to be taken into account.
- Linear convection and linearized radiation boundary conditions can be assumed. Hence, the outward thermal flux from the specimen is proportional to the temperature difference between the surface and the surrounding air, through the boundary conditions constant $h = h_{conv} + h_{rad}$ (W/m^2 °C).
- The bi-dimensional solution for a long body with a rectangular cross section ($2a \times 2b$) can then be determined [30] from the product of two mono-dimensional solutions to the problem of the infinite plate of thickness $2a$ (and $2b$), that is:

$$T\left(\frac{x}{a},Fo\right)=(T_0-T_{amb})\cdot\psi\left(\frac{x}{a},Fo\right)+T_{amb} \quad \text{for } -1\leqslant\frac{x}{a}\leqslant 1, \text{ where} \tag{2}$$

$$\psi\left(\frac{x}{a},Fo\right)=\sum_{k=1}^{\infty}\frac{2\cdot e^{-Fo\cdot\alpha_k^2}}{1+Bi\cdot\left[1+\left(\frac{\alpha_k}{Bi}\right)^2\right]}\cdot\frac{\cos\left(\alpha_k\frac{x}{a}\right)}{\cos(\alpha_k)}=\sum_{k=1}^{\infty}f_k(Fo)\cdot\frac{\cos\left(\alpha_k\frac{x}{a}\right)}{\cos(\alpha_k)} \tag{3}$$

Bi being the Biot number for the thermal transient along the half thickness a:

$$Bi=\frac{h\cdot a}{\lambda} \quad (\lambda=\text{thermal conductivity of concrete}-\text{W/m °C}) \tag{4}$$

and α_k being the roots of the equation:

$$\alpha\tan(\alpha)=Bi \tag{5}$$

As usual in transient thermal problems, the time dependence is governed by the Fourier number (dimensionless time):

$$Fo=\frac{D\cdot t}{a^2} \quad (\text{m}^2/\text{s};\ t=\text{time}). \tag{6}$$

In case the specimen is enclosed in an insulating box at time $\bar{t}$(i.e. $Fo=\bar{Fo}$), the temperature field described by Eq. (2) becomes the initial condition for the second cooling stage, which is controlled by reduced values of the Biot number ($Bi'' < Bi'$) and of the corresponding roots of Eq. (5) ($\alpha_k'' < \alpha_k'$):

$$\psi\left(\frac{x}{a},Fo>\bar{Fo}\right)=\sum_{j=1}^{\infty}\sum_{k=1}^{\infty}f_k'(\bar{Fo})\cdot f_j''(Fo-\bar{Fo})\cdot\frac{\frac{Bi'}{Bi''}-1}{\frac{\alpha_k'^2}{\alpha_j''^2}-1}\cdot\frac{\cos\left(\alpha_j''\frac{x}{a}\right)}{\cos(\alpha_j'')} \tag{7}$$

where functions f_k' and f_j'' are defined as in Eq. (3) for Bi', α_k' and Bi'', α_j'', respectively.

Finally, the bi-dimensional solution for the thermal field within the beam cross section can be expressed as follows for both the cooling stages [30]:

$$T\left(\frac{x}{a},\frac{y}{b},t\right)=(T_0-T_{amb})\cdot\psi_x\left(\frac{x}{a},Fox\right)\cdot\psi_y\left(\frac{y}{b},Foy\right)+T_{amb} \tag{8}$$

and the relative temperature decrease $\Delta T/T < 0$ at any point (x,y) is:

$$\Delta T/T\left(\frac{x}{a},\frac{y}{b},t\right)=\frac{T-T_0}{T_0-T_{amb}}=\left[\psi_x\left(\frac{x}{a},Fox\right)\cdot\psi_y\left(\frac{y}{b},Foy\right)-1\right] \tag{9}$$

where in the general case of the rectangular cross section ($a \neq b$), the Fourier and Biot numbers (and the roots α_k) assume distinct values in the x and y directions.

The accuracy of Eq. (9) in the corner zones has been ascertained via 2D finite element analyses.

A comparison between the two different approaches is shown in Fig. 3a, where the temperature variation of a corner of a $2a \times 2b$ cross section initially at 600 °C is represented according to both the solutions.

Once the convection coefficients have been properly calibrated (Table 2), this model fits pretty well the experimental data concerning the second cooling stage, near the top face of the specimen (Fig. 3). The benefit of the insulating box is noticeable (dashed vs. solid curves) and a temperature drop in the range 10–20% is to be expected at the peak load of the bending tests ($t \cong 2$ min) and a little more during the fiber pull-out phase ($t \leqslant 4$ min).

As regards the self-stress field, it can be assumed that during the cooling process the specimen cross sections keep plane and that no curvature occurs before loading (double symmetry about the x and y axes). Hence, the total longitudinal strain ε_{tot} is a con-stant that can be determined by equating the axial force N to zero:

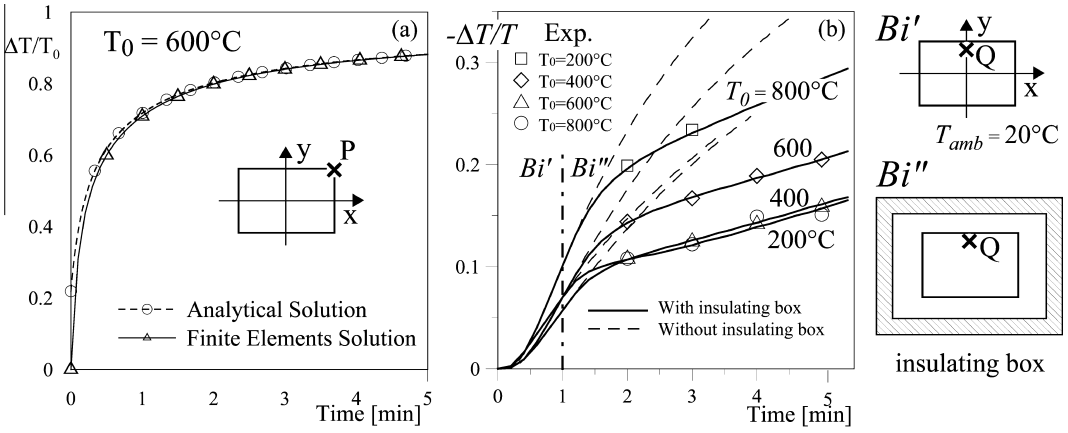

Fig. 3. (a) Comparison between the finite element and the analytical solution without the thermal insulation box. Decrease of temperature vs. time in the corner (point P: $x = 37.5$ mm, $y = 30$ mm); (b) thermal analysis in the middle top fiber (point Q: $x = 0$, $y = 22$ mm) with and without the thermal insulation box.

Table 2
Thermal properties of concrete.

Initial temperature T_0 (°C)	Linear convection and linearized radiation coeff.		Thermal conductivity	Thermal diffusivity
	h' (W/m^2 °C)	h''	λ (W/m °C)	D (10^6 m^2/s)
200	100	25	1.6	0.6
400	110	29	1.2	0.4
600	200	36	0.9	0.3
800	300	50	0.7	0.3

$$N = \int_A \sigma \, dA = \int_A \sigma(\varepsilon_{el}) \, dA = \int_A \sigma(\varepsilon_{\text{tot}} - \beta \cdot \Delta T) \, dA = 0 \qquad (10)$$

where ε_{el} are the elastic strain, β is the thermal strain coefficient (contraction) at the initial material temperature T_0 according to EC2 proposal.

By considering a bi-linear stress-crack opening tensile constitutive law [10,11,31], the mechanical properties decay of T75/50/45 (Fig. 4a) [25,29] and the temperature fields at time $t = 2$ min (bending test peak load), the iso-strain curve corresponding to the incipient cracking condition can be plotted (Fig. 4b). The incipient cracking condition is defined as $\varepsilon = \varepsilon_{ct}^{T_0}$ where $\varepsilon_{ct}^{T_0}$ is the strain at the onset of unstable crack propagation. For sake of simplicity, a linear elastic behavior was considered before the peak in tension $\left(\varepsilon_{ct}^{T_0} = f_{lf}(T_0)/E(T_0)\right)$.

It can be concluded that thermal cracking of the specimen border zone is likely to occur in this hot-testing technique, especially at temperatures higher than 400 °C. However, the crack penetration does not exceed 10–15% of the beam depth. Fig. 5a refers to 800 °C Hot condition for material T75/50/45 and confirms the prediction of the thermal crack penetration. The influence of these cracks is expected to vanish as the bending load approaches the peak. Hence, no significant effects are expected at the peak load and even more during the fiber pull-out phase.

5. Experimental results

The load (P)–deflection (δ) curves presented in Fig. 6 allow us to compare high and low displacement rate tests. In these figures the

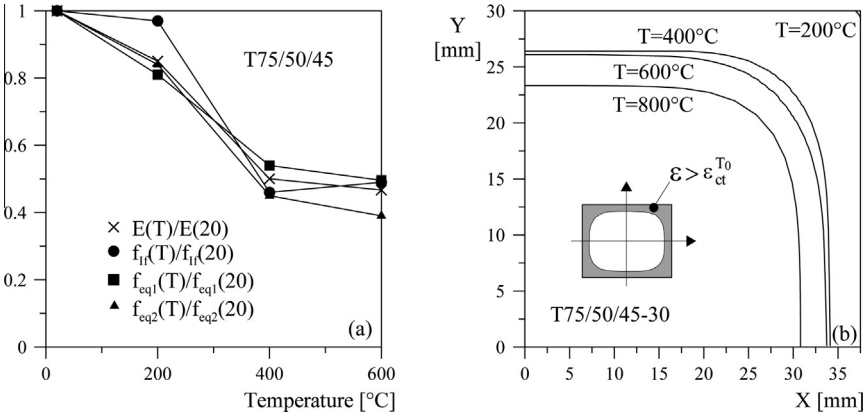

Fig. 4. Decay of the material parameters with temperature (f_{lf} = first cracking strength, f_{eq1} = Serviceability Limit State Strength, f_{eq2} = Ultimate Limit State Strength) [22,26](a) and contour of the incipient cracking due to thermal self-stress (b).

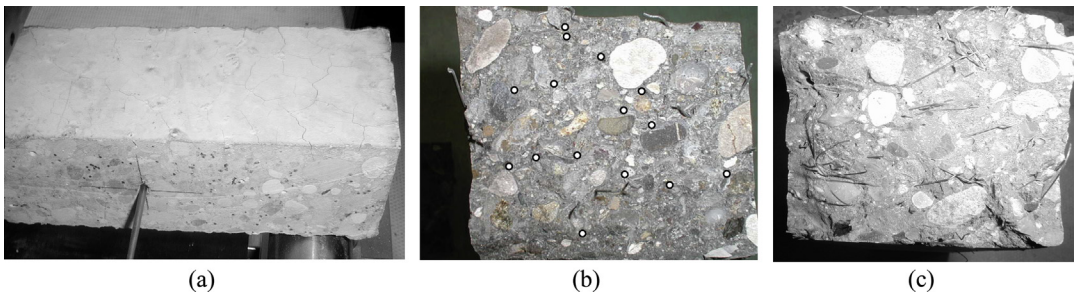

Fig. 5. (a) superficial cracking of specimen of material T75/50/45 after exposure to 800 °C; (b) cross section of a T75/50/45 specimen after testing at 200 °C (c) cross section of a T75/50/45 specimen after testing at 400 °C.

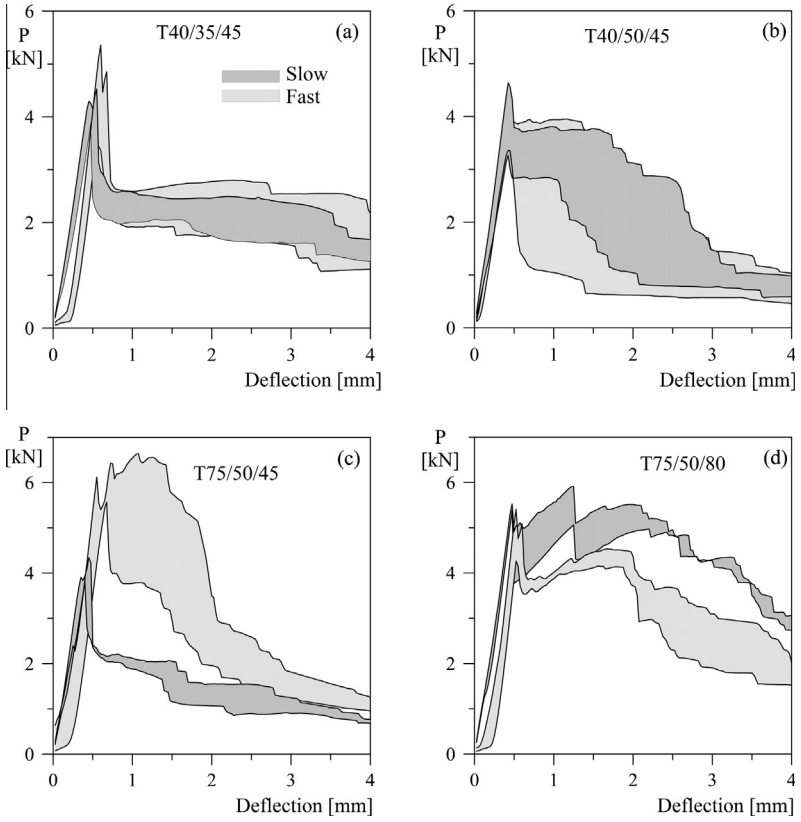

Fig. 6. Comparison between the average curves obtained from slow and fast tests on unheated concrete.

two different regions correspond to the two different deflection rates imposed. In Table 3, a comparison between the two test modalities is carried out by means of the following material strengths:

- Peak strength: nominal stress corresponding to the load peak value.
- f_{eq1}: Serviceability Limit State (SLS) strength evaluated as the average nominal stress in the crack opening range between 3 w_l and 5 w_l according to Italian Design Standards CNR DT 204/05, where w_l is the crack opening corresponding to the first cracking (w_l = 0.1 mm).
- f_{eq2}: Ultimate Limit State (ULS) strength evaluated as the average nominal strength in the crack opening range between 0.8 w_u and 1.2 w_u, where w_u is the ultimate crack opening corresponding to 2% of the specimen depth (w_u = 1.2 mm).

As already discussed, in all "fast" tests, no instruments were used to measure the crack opening; in these cases the kinematic assumption of two rigid bodies was used to evaluate the crack opening considering the load peak as localization point and taking into account the actual crack position for each test. It is worth to note that in all the tests just one crack propagate as shown in Fig. 2a as example. In case of low stroke rate tests, where the crack opening displacements were measured by means of displacement transducers, this hypothesis was validated by computing the same strengths previously discussed (f_{eq1} and f_{eq2}) either considering the measured crack opening ("Slow" column in Table 3) or considering the crack opening calculated by means of the two rigid bodies assumption after cracking ("Slow eval." column in Table 3) for each specimen.

It is evident that the two modalities to evaluate the equivalent strengths are quite similar and the difference is generally lower than 10% with the only exception of two cases in which it can grow up to 20% (T40/50/45; f_{eq2}).

With reference to the deflection rate, the two regions of Fig. 6a and b differ by a quantity which is almost always lower than the scattering observed in each region. This means that the change in

Table 3
Experimental results of the low and high stroke rate tests in room conditions (Slow = slow test strengths calculated with measured COD, Slow eval. = slow test strengths calculated with COD evaluated by means of the rigid bodies assumption, Fast = fast test strengths calculated with COD evaluated by means of the rigid bodies assumption; Scat. = $\max|f_i - f_{av}|/f_{av}$).

Material	Test	Specimen age at test (slow/fast) (d)	Peak strength (N/mm^2)		f_{eq1} (N/mm^2)			f_{eq2} (N/mm^2)		
			Slow	Fast	Slow	Slow eval	Fast	Slow	Slow eval	Fast
T40/35/45	1	453/431	7.25	5.73	3.36	3.34	4.34	2.76	2.98	4.63
	2	453/431	7.64	8.97	4.19	4.25	3.78	4.07	4.12	2.92
	3	453	–	8.10	–	–	3.21	–	–	3.23
	Aver.		**7.44**	**7.60**	**3.78**	**3.79**	**3.77**	**3.42**	**3.55**	**3.60**
	Scat.		**2.68%**	**24.59%**	**11.05%**	**12.03%**	**15.04%**	**19.28%**	**16.07%**	**28.81%**
T40/50/45	1	457/431	7.95	6.32	6.27	6.31	3.59	4.47	5.38	2.20
	2	457/431	5.48	6.59	4.06	4.71	6.52	1.38	1.70	4.86
	3	454	–	6.59	–	–	1.77	–	–	1.04
	Aver.		**6.71**	**6.50**	**5.16**	**5.51**	**3.96**	**2.93**	**3.54**	**2.70**
	Scat.		**18.41%**	**2.71%**	**21.38%**	**14.50%**	**64.57%**	**52.79%**	**51.87%**	**80.11%**
T75/50/45	1	461/401	6.58	9.28	2.83	3.27	6.19	1.51	1.79	3.08
	2	461/401	7.39	11.07	3.51	3.56	9.35	2.57	2.62	4.04
	3	372	–	10.44	–	–	9.73	–	–	3.17
	Aver.		**6.99**	**10.26**	**3.17**	**3.41**	**8.42**	**2.04**	**2.21**	**3.43**
	Scat.		**5.75%**	**9.57%**	**10.60%**	**4.16%**	**26.53%**	**26.02%**	**18.87%**	**17.69%**
T75/50/80	1	313/313	6.45	8.09	8.09	7.85	6.54	6.80	7.61	6.58
	2	313/313	5.94	8.62	7.63	8.32	6.79	5.42	6.29	5.55
	3	297	–	9.05	–	–	6.76	–	–	6.82
	Aver.		**6.19**	**8.59**	**7.86**	**8.09**	**6.70**	**6.11**	**6.95**	**6.31**
	Scat.		**4.09%**	**5.78%**	**2.95%**	**2.86%**	**2.30%**	**11.24%**	**9.45%**	**12.17%**

deflection rate, is negligible only for some materials, even if the small scattering observed for the other materials (T75/50/45, T75/50/80) emphasizes the investigated effect.

The results of tests performed with a high displacement rate are summarized in Fig. 7 by means of the load–deflection (δ) average curves. The most significant result seems to be a good agreement between the hot (H) and residual (R) tests: the corresponding curves show a small difference, which gives an idea of the influence of the actual temperature of the specimen on the behavior of materials, once experienced the damaged introduced in the material for the exposure to the maximum temperature T_0.

Focusing on the behavior of the peak, Tables 4–7 show the differences between the test modalities at each temperature.

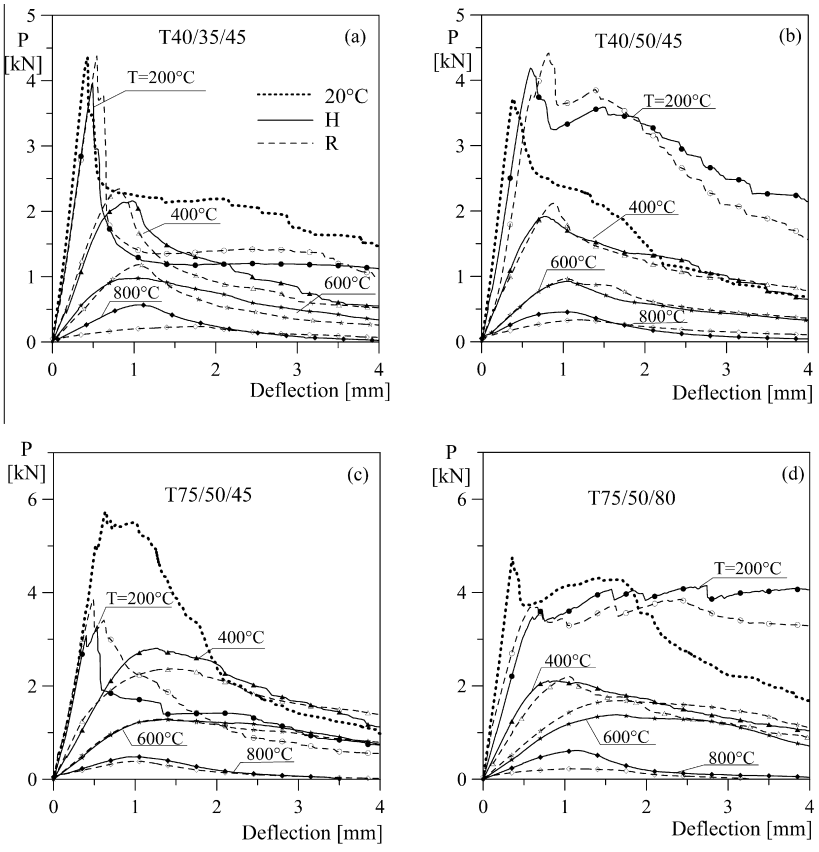

Fig. 7. Average load–vertical displacement (deflection) curves for the four materials investigated.

Table 4
Equivalent strength for thematerial T40/35/45 (scattering = max$|f_i - f_{av}|/f_{av}$).

Temperature (°C)	Test	Specimen age at test (d)		Peak strength (N/mm^2)		f_{eq1} (N/mm^2)		f_{eq2} (N/mm^2)	
		Hot	Residual	Hot	Residual	Hot	Residual	Hot	Residual
200	1	455	457	6.80	8.74	1.68	2.53	1.58	2.57
	2	455	457	7.02	7.56	2.61	2.96	2.39	3.47
	3		457		7.02		1.56		0.98
	Average			**6.91**	**7.77**	**2.15**	**2.35**	**1.99**	**2.34**
	Scattering			**1.58%**	**12.45%**	**21.59%**	**33.75%**	**20.53%**	**57.93%**
400	1	448	450	3.81	3.81	3.32	2.65	2.02	2.03
	2	448	450	3.76	4.38	1.34	1.88	0.88	1.16
	3	448	450	3.47	3.68	2.87	1.87	2.04	1.05
	Average			**3.68**	**3.96**	**2.51**	**2.13**	**1.65**	**1.41**
	Scattering			**5.65%**	**10.67%**	**46.64%**	**24.25%**	**46.54%**	**43.55%**
600	1	453	455	1.49	1.89	1.46	1.33	1.12	0.73
	2	453	455	1.85	1.94	1.57	1.07	0.89	0.58
	3	453	455	1.68	2.16	1.42	1.39	0.83	0.89
	Average			**1.67**	**2.00**	**1.49**	**1.26**	**0.95**	**0.73**
	Scattering			**10.83%**	**8.21%**	**5.84%**	**15.43%**	**18.62%**	**21.99%**
800	1	462	464	1.01	0.35	0.63	0.31	0.25	0.22
	2	462	464	1.05	0.57	0.74	0.32	0.29	0.16
	3	462	464	0.79	0.42	0.51	0.36	0.14	0.24
	Average			**0.95**	**0.44**	**0.63**	**0.33**	**0.23**	**0.21**
	Scattering			**16.75%**	**28.09%**	**18.50%**	**7.77%**	**37.86%**	**21.60%**

Table 5
Equivalent strength for the material T40/50/45 (scattering = max$|f_i - f_{av}|/f_{av}$).

Temperature (°C)	Test	Specimen age at test (d)	Specimen age at test (d)			f_{eq1} (N/mm^2)		f_{eq2} (N/mm^2)	
		Hot	Hot	Hot	Residual	Hot	Residual	Hot	Residual
200	1	466	468	7.33	7.73	4.23	5.54	3.87	5.09
	2	466	468	7.88	8.69	7.48	5.50	5.57	4.37
	3	466	468	7.45	8.81	5.46	7.70	4.98	5.30
	Average			**7.55**	**8.41**	**5.72**	**6.25**	**4.81**	**4.92**
	Scattering			**4.29%**	**8.07%**	**30.76%**	**23.34%**	**19.39%**	**11.09%**
400	1	449	451	3.66	3.28	3.28	2.00	3.21	1.39
	2	449	451	3.40	3.56	2.65	2.30	1.79	1.93
	3	449	451	2.74	3.78	2.00	3.03	1.39	2.13
	Average			**3.27**	**3.54**	**2.64**	**2.45**	**2.13**	**1.82**
	Scattering			**16.10%**	**7.30%**	**24.22%**	**23.79%**	**50.83%**	**23.43%**
600	1	454	456	2.01	1.97	1.56	1.10	1.08	0.80
	2	454	456	1.89	1.09	1.19	0.96	0.73	0.74
	3	454	456	0.86	2.33	0.75	1.52	0.63	0.90
	Average			**1.59**	**1.80**	**1.17**	**1.19**	**0.81**	**0.81**
	Scattering			**45.92%**	**39.21%**	**35.71%**	**27.13%**	**32.78%**	**10.90%**
800	1	462	464	0.65	0.56	0.47	0.43	0.19	0.25
	2	462	464	0.96	0.54	0.62	0.45	0.26	0.33
	3	462	464	0.78	0.60	0.60	0.45	0.14	0.26
	Average			**0.80**	**0.57**	**0.56**	**0.45**	**0.20**	**0.28**
	Scattering			**20.32%**	**5.34%**	**16.59%**	**2.99%**	**32.89%**	**18.33%**

It is worth noting that steel macrofibers used do not affect peak strength, but rather the post-peak behavior. This means that the values shown in the figure give us a measure of how the two procedures influence the matrix strength. The difference between the test procedures, when compared with the scattering recorded for each nominally identical test (up to 39%), is significant only for the highest temperature considered (T = 800 °C). In this case, the peak residual strength is in favor of safety as known for plain con-crete data available from the literature [32].

In the post-peak behavior the difference highlights that residual test condition is not always on the safe side. It is worth noting that post-cracking residual strengths are not usually indicated even in recent and outstanding papers [33].

In order to understand the above evidence better, Tables 4–7 also summarize the test results for all the specimens investigated in terms of the material post-peak equivalent strengths previously discussed (f_{eq1} and f_{eq2}), as suggested by the Italian Design Standard for FRC Structures.

It is important to point out that the investigated materials show a high scattering of the results. This is a peculiarity of SFRC which is usually characterized by a variation coefficient equal to 15% and 25% for SLS and ULS respectively [3]. By considering three specimens for each test, the maximum distance of the results from the average value, normalized by the average value itself, assumes the values of 51% and 85% respectively for SLS and ULS when a Gaussian distribution is taken into account (k = 3.4 for n = 5).

In order to weigh better the difference between the two testing modalities (H and R) a strength and a toughness criteria were introduced. The maximum load difference at a given displacement (δ) among the three nominally identical repeated tests performed for each case (defined in Fig. 9a and named hot and residual in Figs. 10–13) is compared with the load difference between the

Table 6
Equivalent strength for the material T75/50/45 (scattering = max$|f_i - f_{av}|/f_{av}$).

Temperature (°C)	Test	Specimen age at test (d)		Peak strength (N/mm^2)		f_{eq1} (N/mm^2)		f_{eq2} (N/mm^2)	
		Hot	Residual	Hot	Residual	Hot	Residual	Hot	Residual
200	1	536	538	6.38	7.61	2.76	2.30	2.08	1.42
	2	536	538	5.93	7.58	1.10	4.18	1.11	2.27
	3	536	538	6.38	7.06	4.64	4.27	3.88	1.78
	Average			**6.23**	**7.42**	**2.83**	**3.58**	**2.35**	**1.82**
	Scattering			**4.81%**	**4.85%**	**63.62%**	**35.84%**	**64.72%**	**24.66%**
400	1	463	466	5.19	4.62	4.11	4.20	2.49	3.04
	2	463	466	4.67	3.37	4.11	2.95	3.29	2.23
	3	463	466	4.50	4.03	3.68	3.38	2.68	2.67
	Average			**4.79**	**4.01**	**3.97**	**3.51**	**2.82**	**2.65**
	Scattering			**8.50%**	**15.85%**	**7.25%**	**19.68%**	**16.63%**	**15.64%**
600	1	367	364	2.65	2.07	2.54	1.76	2.49	1.21
	2	367	364	1.87	2.45	1.64	2.36	1.55	1.97
	3	367	364	2.02	1.97	1.97	1.87	1.40	1.62
	Average			**2.18**	**2.16**	**2.05**	**1.99**	**1.81**	**1.60**
	Scattering			**21.65%**	**13.22%**	**23.80%**	**18.26%**	**37.23%**	**24.21%**
800	1	534	536	0.91	0.80	0.65	0.34	0.14	0.11
	2	534	536	0.97	0.55	0.64	0.43	0.21	0.16
	3	534	536	0.73	0.73	0.51	0.47	0.17	0.18
	Average			**0.87**	**0.70**	**0.60**	**0.41**	**0.17**	**0.15**
	Scattering			**15.83%**	**20.40%**	**14.18%**	**18.34%**	**20.68%**	**25.05%**

Table 7
Equivalent strength for the material T75/50/80 (scattering = max$|f_i - f_{av}|/f_{av}$).

Temperature (°C)	Test	Specimen age at test (d)		Peak strength (N/mm^2)		f_{eq1} (N/mm^2)		f_{eq2} (N/mm^2)	
		Hot	Residual	Hot	Residual	Hot	Residual	Hot	Residual
200	1	313	301	8.01	7.15	7.66	6.52	7.18	5.65
	2	297	301	5.93	6.88	5.32	6.69	4.91	5.11
	3	297	301	8.28	5.81	7.46	4.71	6.47	4.03
	Average			**7.41**	**6.61**	**6.81**	**5.97**	**6.19**	**4.93**
	Scattering			**19.91%**	**12.12%**	**21.97%**	**21.21%**	**20.65%**	**18.33%**
400	1	315	517	3.40	4.82	2.87	2.85	2.18	1.30
	2	315	517	3.80	2.62	3.20	2.60	2.78	2.04
	3	315	318	3.72	3.96	3.13	3.33	2.37	2.62
	Average			**3.64**	**3.80**	**3.07**	**2.93**	**2.45**	**1.99**
	Scattering			**6.61%**	**31.04%**	**6.49%**	**13.90%**	**13.79%**	**34.48%**
600	1	456	289	2.38	2.89	2.08	2.76	1.98	2.14
	2	456	289	2.58	2.53	2.20	2.21	1.43	1.72
	3	292	289	2.02	3.18	1.88	3.07	1.40	2.35
	Average			**2.33**	**2.87**	**2.06**	**2.68**	**1.60**	**2.07**
	Scattering			**13.21%**	**11.83%**	**8.61%**	**17.47%**	**23.20%**	**16.68%**
800	1	517	519	0.99	0.61	0.63	0.29	0.29	0.10
	2	517	519	1.16	0.38	0.50	0.27	0.13	0.11
	3	517	519	1.04	0.32	0.64	0.22	0.15	0.05
	Average			**1.06**	**0.44**	**0.59**	**0.26**	**0.19**	**0.09**
	Scattering			**9.40%**	**39.28%**	**15.23%**	**15.02%**	**53.02%**	**38.51%**

average curves of each procedure at the same displacement (δ) (defined in Fig. 9b and named average *H–R* in Figs. 10–13).

The comparison, shown in Figs. 10–13 for all the materials, underlines how the difference between the two test modalities is generally lower than the maximum scattering registered in each homogeneous group of tests for all the temperatures investigated; the only exception is the maximum temperature of 800 °C.

The same conclusion is also confirmed in Table 8, where, for each material, the maximum local difference between the three nominally identical tests (Fig. 9a) is compared with the maximum local difference between the two average curves of the hot and residual conditions (Fig. 9b). In these tables the same comparison is also performed by considering toughness measured as the whole area subtended by the load–displacement (δ) curves as defined in Fig. 9c and 9d. As already discussed, the difference between the two test modalities is greater than the scattering of the materials themselves just in the case of 800 °C.

The careful analysis of all this extended database allows us to conclude that, for this kind of materials reinforced with steel macro-fibers, the residual procedure can be adopted in order to evaluate post-peak mechanical parameters decay when exposed to high temperature.

The decay of the average equivalent strengths at increasing temperatures is summarized in Fig. 8.

The resulting curves show different evolutions which can locally differ from EC2 linear decay proposal for plain concrete up to 100%. First of all, all the materials exhibit a smaller strength decay with respect to that proposed for plain concrete for temperatures higher than 400 °C.

For each material the mechanical parameters do not show the same trend, thus resulting a wider fan of curves. The main difference between the material responses is observable in the range 200 –400 ° C which is generally the most interesting for structures exposed to fire.

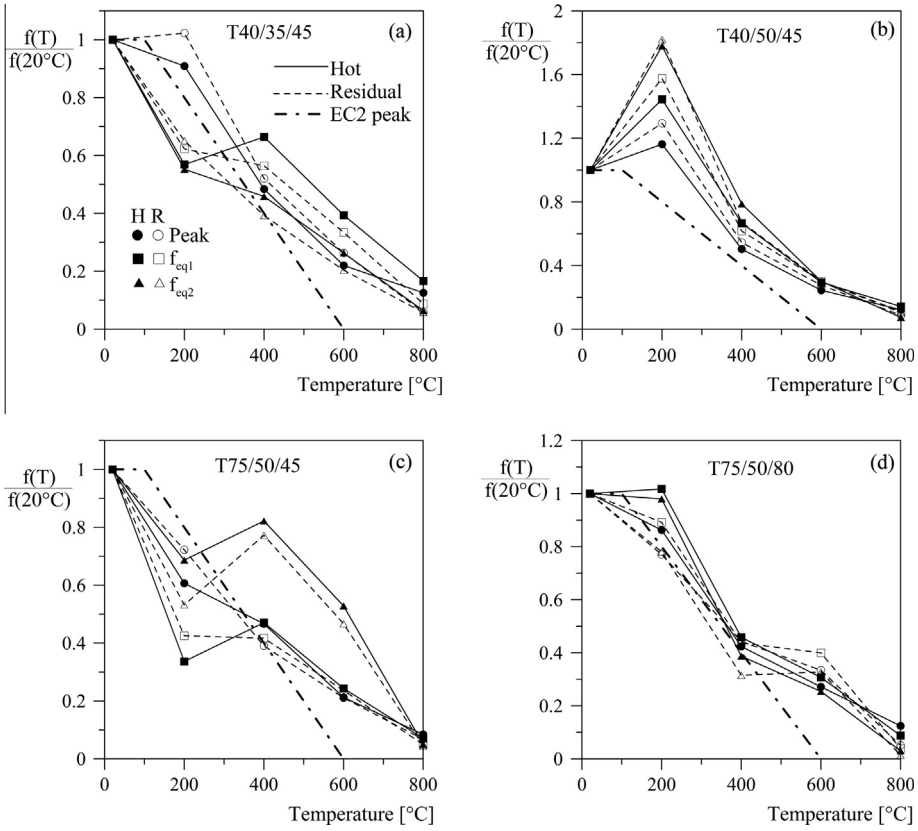

Fig. 8. Equivalent strength vs. temperature curves for the four materials investigated.

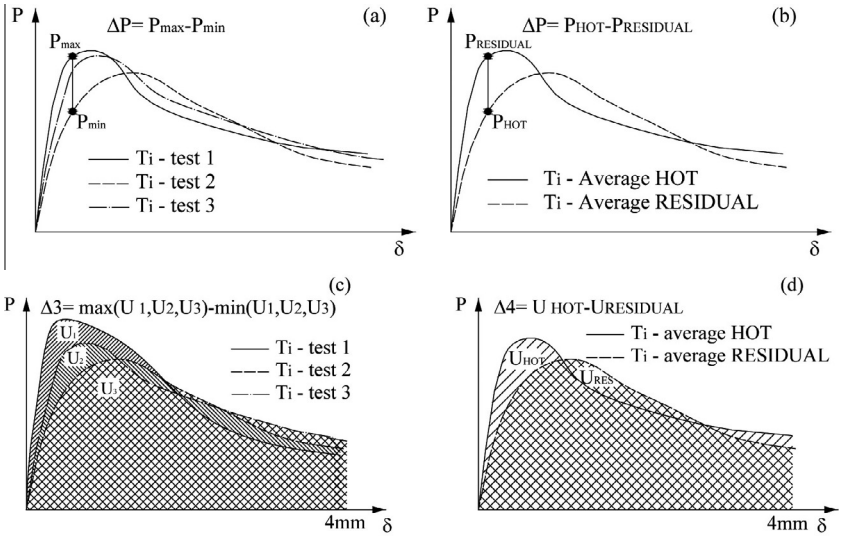

Fig. 9. Definition of local scattering: (a) between nominally identical tests and (b) between different testing modalities (hot vs. residual); definition of area scattering: (c) between nominally identical tests and (d) between different testing modalities (hot vs. residual).

Moreover, some specific observations worth to be discussed. T75/50/45 material shows at 200 °C lower strength with respect to the T40/50/45 even if it is characterized by the same fiber type and content and a lower compressive strength of the matrix. This is mainly related to the high strength of the matrix for which low carbon steel fibers used cannot activate the pull-out mechanism due to the failure of the fiber itself. The effect is emphasized at 200 °C because of the bond strength increase at that temperature thanks to the drying shrinkage action. The same effect does not occur for higher temperatures due to thermal damage introduced into the matrix caused by the heterogeneity of the matrix itself. A picture of the T75/50/45 failure cross section respectively at 200 °C and 400 °C is repre-sented respectively in Fig. 5b and c: in Fig. 5b the position of the broken fibers is highlighted by white points on the cross section.

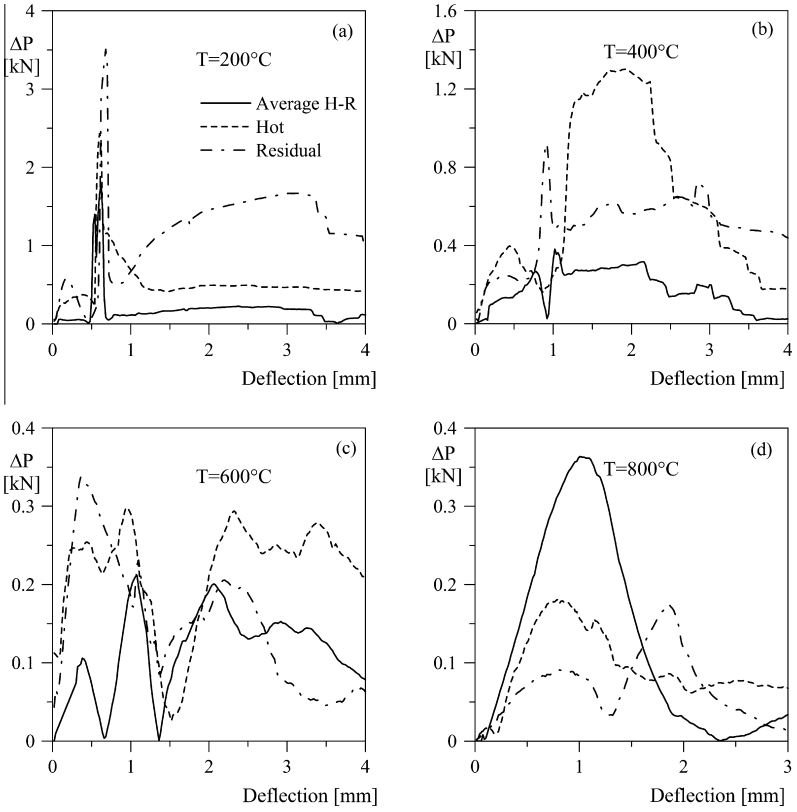

Fig. 10. Scattering comparison for material T40/35/45.

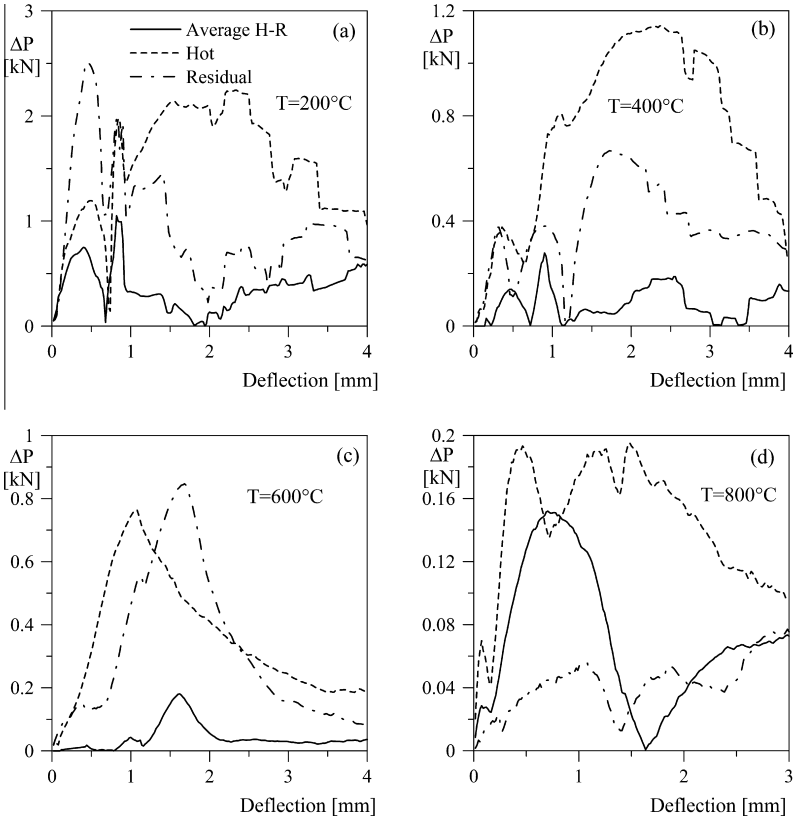

Fig. 11. Scattering comparison for material T40/50/45.

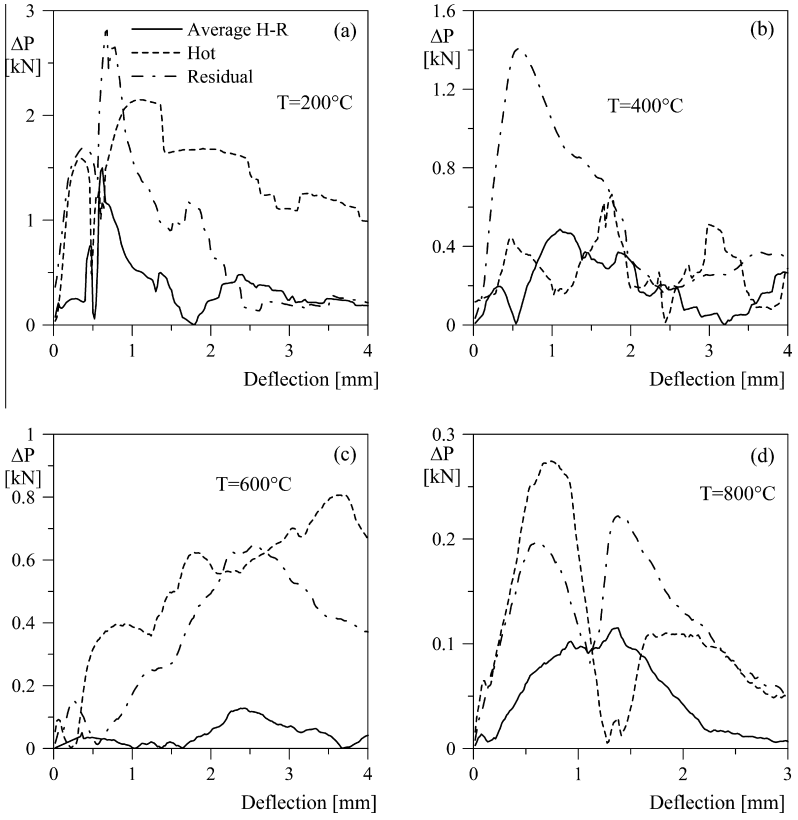

Fig. 12. Scattering comparison for material T75/50/45.

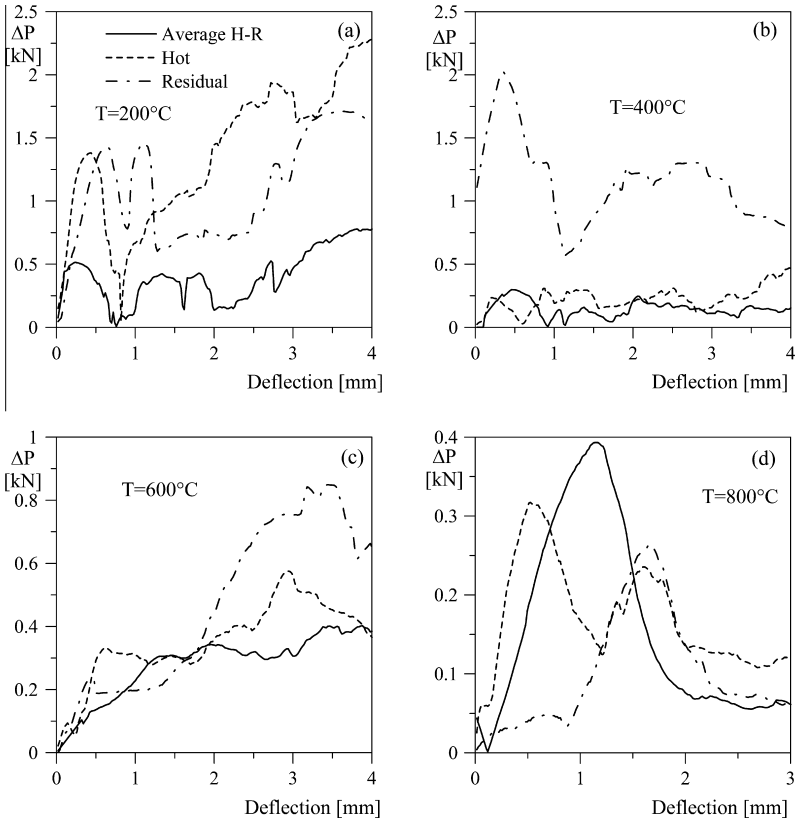

Fig. 13. Scattering comparison for material T75/50/80.

Table 8
Scattering of the tests for different materials.

Material	Temperature (°C)	Δ1 (kN)		Δ2 (kN)	Δ3 (kN m)		Δ4 (kN m)
		Hot	Residual		Hot	Residual	
T40/35/45	200	2.43	3.51	1.79	1.76	4.47	−0.66
	400	1.30	0.92	0.38	2.27	1.85	0.44
	600	0.30	0.34	0.21	0.51	0.57	0.31
	800	0.18	0.17	0.36	0.28	0.07	0.36
T40/50/45	200	2.25	2.51	1.05	4.99	2.89	0.69
	400	1.14	0.67	0.28	2.76	1.33	0.13
	600	0.76	0.85	0.18	1.42	1.06	−0.17
	800	0.20	0.08	0.15	0.27	0.05	0.08
T75/50/45	200	2.15	2.81	1.50	5.41	1.79	−0.22
	400	0.66	1.41	0.49	0.27	2.26	0.38
	600	0.81	0.65	0.13	1.85	1.31	0.08
	800	0.27	0.22	0.12	0.13	0.12	0.16
T75/50/80	200	2.28	1.71	0.78	5.14	3.87	1.29
	400	0.47	2.03	0.30	0.70	1.49	0.55
	600	0.58	0.85	0.40	1.41	1.85	−1.12
	800	0.32	0.26	0.39	0.04	0.28	0.47

Δ1: Maximum local scattering between nominally identical curves (max ΔP defined in Fig. 9a). Δ2: Maximum local scattering between average hot and residual curves (max ΔP defined in Fig. 9b). Δ3: Maximum area scattering between nominally identical curves (ΔU defined in Fig. 9c).
Δ4: Maximum area scattering between average hot and residual curves (ΔU defined in Fig. 9d).

Also in the case of T40/50/45, the drying shrinkage action at 200 °C favors both the stable and unstable crack propagations leading to higher equivalent strengths with respect to those obtained at 20 °C.

It is worth noting that the post-cracking strength of T75/50/45 at 400 °C are generally higher than those at 200 °C: this can be related to the fact that the concrete matrix strength is more sensitive than pull-out strength to thermal damage and this induces a smaller peak strength that implies a smaller energy release rate due to the crack propagation, thus showing a larger ductility.

At the same time at 400 °C the higher strength observed for the material T75/50/45 with respect to those of T75/50/80 is due to the different fiber types for which the percentage of cross section reduction consequent to oxidation is much larger on the small fiber cross-section with respect to the large fiber diameter. Moreover, high carbon fiber are much more sensitive to thermal damage compared to low carbon fiber.

Finally, the investigation carried out allows us to highlight the reliability of the experimental procedure adopted thanks to the following considerations:

1. During the hot test, the cooling process of the specimen is quite well controlled by the insulating thermal box. The specimen has a temperature decrease of about 15% of the initial temperature on its external face in the whole duration of the test.
2. Considering thermal self-stresses due to fast extraction from the furnace, it can be seen that they affect only the first initial elastic behavior of the specimen, with no significant consequences on the post-peak behavior.
3. The displacement rate investigated ranged between 0.1 mm/min to 1 mm/min in the pre-peak phase and from 0.25 mm/min to 2 mm/min in the post-peak phase. The results show how the deflection rate effect cannot be considered always negligible, thus depending on the material investigated. Nevertheless, the change in deflection rate is negligible when compared to the scattering observed in nominally identical tests for each material: this was expected since all the deflection rates considered stand in the quasi-static domain.

6. Conclusions

The identification of the mechanical parameters carried out at room temperature after a suitable thermal exposure of the specimens can be proposed as a reliable procedure. It is aimed at computing the residual bearing capacity after a fire event by using residual mechanical properties; it can even be used to predict the structure resistance during fire, because very often it is in favor of safety in relation to the displacement rate applied, and it has been demonstrated that there are not significant differences between hot and residual conditions, at least for the highest displacement rate considered.

On the basis of the test results obtained, the following remarks on the objectives pointed out in the introduction can be formulated:

a. The comparison between residual and hot tests highlights that the test procedure has a negligible contribution on the results. Hence, the mechanical behavior of SFRC at high temperatures is mainly governed by the maximum temperature experienced by the material. The agreement between the two test modalities is confirmed all the more if compared with the scattering of the results obtained in each procedure.
b. The decay curves of SFRC materials investigated always exhibit a better behavior with respect to plain concrete for temperatures higher than 400 °C. For lower temperatures a no unique trend was observed. It is worth noting that the present results are limited to the temperature lower than 800 °C and also to the steel fiber content considered (up to 50 kg/m^3); further investigations are needed when a higher fiber content is considered as for instance for HPRFC materials.
c. Looking at the results for the four different materials investigated, it is not possible to define a unique degradation function that does not depend on the specific SFRC; therefore a proper identification procedure is needed for each material when the fire design of the structure is required. For temperatures higher than 400 °C the degradation proposed by EC2 for plain concrete can be used being always

on the safe side. The paper presents a proper procedure to identify the specific residual strength variation for a general SFRC material that can be used in fire design of structural elements uncoupling the thermal and the mechanical behavior of the structure.

d. The tests carried out do not allow us a correct measure of the bond strength reduction with thermal damage. The parameter that mainly relates to bond strength is the equivalent strength computed for small crack opening values when the hooked-end contribution is less effective. Looking at the failure state of the specimen, the pull-out mechanism prevails even at the highest temperature. The only exception was observed for T75/50/45 at 200 °C that exhibited a brittle post peak behavior.
e. The materials investigated can basically be considered as brittle because they never present a multicrack pattern. For temperatures up to 200 °C this brittleness can even be increased by the positive effect of shrinkage on the peak due to bond increase. For temperatures higher than 400 °C the thermal damage affects more the matrix behavior rather than pull-out effect, thus leading to a more ductile global response.

Acknowledgements

The authors thank Magnetti Larco-Building for the technical support in the experimental investigation and M.S. Claudio Failla for the direction of the experimental investigation carried out.

References

[1] di Prisco M, Felicetti R. HSC thin-web roof-elements: an experimental investigation on steel fibre benefits. In: Proceedings of the 5th Int. Symposium on utilization of high strength/high performance concrete, Sandefjord, Norway, 1999. p. 546–55.
[2] Sernà P, Arango S, Ribeiro T, Núñez AM, Garcia-Taengua E. Structural cast-in-place SFRC: technology, control criteria and recent applications in Spain. Mater Struct 2009;42:1233–46.
[3] di Prisco M, Plizzari G, Vandewalle L. Fibre reinforced concrete: new design perspectives. Mater Struct 2009;42:1261–81.
[4] di Prisco M, Colombo M. FRC thin walled structures: opportunities and threats. In: Barros et al., editors. Fibre reinforced concrete: challenges and opportunities, Proc of the 8th RILEM international symposium BEFIB 2012. RILEM Publications S.A.R.L.; 2012. p. 23–49.
[5] Lappa ES, van der Veen C, Walraven JC. Self-Compacting, high-strength steel fibre-reinforced mortar for precast sheet piles. In: Wallevik O, Nielsson I, editors. Proceeding 3rd Int. Rilem Symp. on SCC. Bagneux: RILEM Publications SARL; 2003. p. 732–40.
[6] Trottier JF, Banthia N. Toughness characterization of steel-fiber reinforced-concrete. J Mater Civ Eng 1994;6:264–89.
[7] Bentur A, Mindness S. Fiber reinforced cementitious composites. Elsevier; 1990.
[8] Reinhardt HW, Naaman AE. High Performance Fiber Reinforced Cement Composites (HPFRCC5). In: Proceeding of the fifth international RILEM workshop PRO 53. Bagneux: RILEM Publications S.A.R.L.; 2007.
[9] EN 14651, Test method for metallic fibered concrete – Measuring the flexural tensile strength.
[10] di Prisco M, Colombo M, Dozio D. Fibre-reinforced concrete in fib Model Code 2010: principles, models and test validation. Struct Concr 2013;14(4):342–61.
[11] di Prisco M, Felicetti R, Lamperti M, Menotti G. On size effect in tension of SFRC thin plates. In: Li VC et al., editors. Fracture mechanics of concrete structures, vol. 2. USA: B.L. Schmick and A.D. Pollington; 2004. p. 1075–82.
[12] di Prisco M, Felicetti R, Iorio F. Il comportamento flessionale di elementi sottili in HPC. In: di Prisco M, Plizzari G, editors. La meccanica della frattura nel calcestruzzo ad alte prestazioni. Brescia: Starrylink; 2003. p. 157–82 (in Italian).
[13] di Prisco M, Dozio D, Belletti B. On the fracture behaviour of thin-walled SFRC roof elements. Mater Struct 2013;46(5):803–29.
[14] Soroushian P, Lee CD. Distribution and fibre orientation of fibers in steel fiber reinforced concrete. ACI Mater J 1990;87:433–9.
[15] Ferrara L, Meda A. Relationships between fibre distribution, workability and the mechanical properties of SFRC applied to precast roof elements. Mater Struct 2006;39:411–20.
[16] Felicetti R, Gambarova PG, Natali Sora MP, Khoury GA. Mechanical behaviour of HPC and UHPC in Direct tension at high temperature and after cooling. In: Rossi P, Chanvillard G, editors. Proceeding 5th symposium on fibre-reinforced concrete BEFIB. Cachan: RILEM Publications S.A.R.L.; 2000. p. 749–58.
[17] Bamonte P, Felicetti R. High-temperature behaviour of concrete in tension. Struct Eng Int 2012;22(4):493–9.
[18] Felicetti R, Gambarova PG. On the residual tensile properties of high-performance siliceous concrete exposed to high temperature. In: Pijaudier-Cabot G, Bittnar Z, Gérard B, editors. Mechanics of quasi-brittle materials and structures. Paris: HERMES Science Publications; 1999. p. 167–86.
[19] Pimienta P. Évolution des caractéristiques des BHP soumis à des températures élevées: Résistances en compression et modules d'élasticité. Cahiers du CSTB; 2001. p. 3353 (in French).
[20] Piti S, Worachet P, Smith S. Post-crack (or post-peak) flexural response and toughness of fiber reinforced concrete after exposure to high temperature. Constr Build Mater 2010;24(10):1967–74.
[21] Poon CS, Shui ZH, Lam L. Compressive behavior of fiber reinforced high-performance concrete subjected to elevated temperature. Cem Concr Res 2004;34(12):2215–22.
[22] Lau A, Anson M. Effect of high temperature on high performance steel fibre reinforced concrete. Cem Concr Res 2006;36:1698–707.
[23] Lie TT, Kodur VR. Thermal and mechanical properties of steel–fibre-reinforced concrete at elevated temperatures. Can J Civ Eng 1996;23(4):511–7.
[24] di Prisco M, Iorio F, Plizzari G. HPFRC prestressed roof elements. In: Shnutgen B, Vandewalle L, editors. Test and design methods for steel fibre reinforced concrete – background and experiences. Bagneux: RILEM Publications S.A.R.L; 2003. p. 161–88.
[25] di Prisco M, Felicetti R, Gambarova PG, Failla C. On the fire behavior of SFRC and SFRC structures in tension and bending. In: Naaman AE, Reinhardt HW, editors. High Performance Fiber Reinforced Cement Composites HPFRCC4, Proc. 4th International RILEM Workshop PRO 30. Bagneux: RILEM Publications S.A.R.L.; 2003. p. 205–20.
[26] EN 1992-1-2. Eurocode 2: design of concrete structures. Part 1. 2: General rules – structural fire design, 2004.
[27] UNI 9502. An analytical procedure to assess the fire resistance of R/C and P/C elements, Italian institute of standards; 2001.
[28] Felicetti R, Ferrara L. The effect of steel fibre on concrete conductivity and its relation to on-site material assessment. In: Gettu R, editor. Proc. of seventh international RILEM symposium on fibre reinforced Concrete: design and application. Bagneux: RILEM Publications S.A.R.L.; 2008. p. 525–35.
[29] Colombo M, di Prisco M, Felicetti R. Mechanical properties of steel fibre reinforced concrete exposed at high temperatures. Mater Struct 2010;43:475–91.
[30] Carslaw HS, Jaeger JC. Conduction of heat in solids. Oxford University Press; 1959.
[31] FIB Model Code 2010, fib bulletin 55 & 56, FIB – Féd. Int. du Béton; 2010.
[32] Abramowicz, M.; Kowalski, R. 2007. Residual mechanical material properties for the reassessment of reinforced concrete structures after fire. In M.J.Skibniewski, P. Vainiūnas, E.K. Zavadskas (eds) The 9th International conference,Modern building materials, structures and techniques. Selected papers, vol. 3. May 16-18,2007, Vilnius, Lithuania. Vilnius: Technika, p. 1147–1151.
[33] Khaliq W, Kodur V. Thermal and mechanical properties of fiber reinforced high performance, self-consolidating concrete at elevated temperatures. Cem Concr Res 2011;41(2011):1112–22.